Effects of chemical absorption on mass transfer from single carbon dioxide bubbles in aqueous sodium hydroxide solution in a vertical pipe

Sa'adiyah, Devy Setiorini ; Matsuo, Yuki ; Schlueter, Michael ; Kurimoto, Ryo ; Hayashi, Kosuke ; Tomiyama, Akio

(Citation)
Chemical Engineering Science,245:116852

(Issue Date)
2021-12-14

(Resource Type)
journal article

(Version)
Accepted Manuscript

(URL)
https://hdl.handle.net/20.500.14094/90008695

Title: Effects of chemical absorption on mass transfer from single carbon dioxide bubbles in aqueous sodium hydroxide solution in a vertical pipe

Authors: Devy Setiorini Sa'adiyah[a], Yuki Matsuo[a], Michael Schlüter[b], Ryo Kurimoto[a], Kosuke Hayashi[a], Akio Tomiyama[a]*

Affiliation: [a] Graduate School of Engineering, Kobe University

[b] Institute of Multiphase Flows, Hamburg University of Technology

*Corresponding author:

Akio Tomiyama

Department of Mechanical Engineering

Graduate School of Engineering

Kobe University

Address: 1-1 Rokkodai, Nada, Kobe, 657-8501, Japan

Tel. & Fax: +81-78-803-6131

e-mail address: tomiyama@mech.kobe-u.ac.jp

Abstract

Mass transfer rates k_L of single carbon-dioxide bubbles with chemical absorption in a vertical pipe were investigated using aqueous sodium hydroxide solutions. The pH of the solution was varied from 12 to 13.15. The pipe diameter D was 12.5 mm. The bubble diameter d was varied for $0.4 < d/D < 1.4$ to cover various bubble shapes. The enhancement factor, E, which is the ratio of k_L with and without chemical absorption, was almost unity for pH < 12.25. Then E increased with increasing pH and d for pH > 12.25. Its magnitude was, however, lower than the estimation by the two-film theory. An E correlation was developed. Good estimation of the Sherwood number for bubbles with chemical absorption was obtained by combining the E correlation and the Sherwood number correlations for bubbles without chemical absorption. Applicability of the correlations to bubbles in a larger pipe diameter was also examined.

Keywords: CO_2 bubble; Sodium hydroxide (NaOH); Chemical absorption; Enhancement factor

1. Introduction

The growth in CO_2 emission is still high as fossil fuels are still the primary fuel for power plants. Many techniques have been developed to reduce CO_2 emission, for example, post-combustion CO_2 capture using chemical absorption by wet scrubber, bubble column reactor, and gas absorber (Mondal et al., 2012; Shim et al., 2016). The concept is uncomplicated; flue gas with CO_2 purged into a reactive solvent changes to other ions. Many solvents have been examined to obtain the maximum efficiency of CO_2 removal, and sodium hydroxide (NaOH) has the highest removal percentage, 92–99% (Peng et al., 2012).

Despite the basic principle of CO_2 removal using chemical absorption, the design of bubble column reactors needs many considerations, including fundamental design data, e.g., physicochemical properties, mass transfer coefficients, and enhancement factors *E*. The latter is a dimensionless number used to define how faster the absorption rate by using chemical absorption is compared to the physical absorption (Danckwerts, 1970):

$$E = \frac{k_L}{k_L^0} = \frac{Sh}{Sh^0} \tag{1}$$

where k_L and k_L^0 are the mass transfer coefficients with and without chemical absorption, respectively, and Sh and Sh^0 are the Sherwood numbers with and without chemical absorption.

Most of the studies on CO_2 absorption in NaOH solutions have been carried out for flows in bubble column reactors, both experimental and numerical (Fleischer et al., 1996; Schulzke et al., 1998; Darmana et al., 2005; Darmana et al., 2007; Sujatha et al., 2017; Krauβ and Rzehak, 2017; Krauß and Rzehak, 2018). The numerical simulation implemented an enhancement factor based on an analytical approximation derived from several enhancement factor theories, such as the penetration (Hikita et al., 1972; DeCoursey, 1974), the surface renewal (DeCoursey, 1974), and the two-film theories (van Krevelen and Hoftijzer, 1948a; Hikita and Asai, 1976). Fleischer et al. (1996) used the two-film theory to estimate *E* for different

concentrations of NaOH ($7 \leq pH \leq 14$). They obtained E as a function of pH and implemented it into the numerical simulation for bubbly flows. Basically, the theoretical derivations of E considered only the rate of diffusion through a flat interface. The bubble column reactor is however a multi-bubble system including a wide range of bubble diameter. The flat interface assumption cannot be adopted unless the radius of the interface curvature is infinitely large. Hence, it is required to obtain knowledge on mass transfer with chemical reactions from single bubbles of various diameters and shapes.

Madhavi et al. (2007) experimentally observed a single spherical CO_2 bubble rising through infinite stagnant NaOH aqueous solutions at 4, 6, and 10 w/v% in the range of bubble diameter from 0.45 to 0.65 mm. The experiments showed that the bubble diameter decreased significantly as the NaOH concentration increased, i.e. the increase in the NaOH concentration enhanced the mass transfer. This tendency was well reproduced by a prediction model taking into account E (Brian et al., 1961). Jia and Zhang (2017) used the experimental results by Madhavi et al. for comparison with their numerical predictions. Their simulation showed that the chemical reaction dominated the local mass transfer rate. The chemical absorption from Taylor bubbles was studied by Kundu et al. (2012), who focused only on the percentage of removed CO_2 during experiments with different pipe diameters and NaOH concentrations. To this point, our knowledge on the chemical absorption of deformed bubbles is insufficient. In particular, there is no experimental evidence on the relationship between E and pH for single bubbles proposed by Fleischer et al.

In this study, experiments of single CO_2 bubbles with various shapes were carried out with several NaOH concentrations to obtain k_L of the chemical absorption. The mass transfer coefficients were compared with those of the physical absorption k_L^0 obtained in our previous study (Hosoda et al, 2014) to evaluate E. An empirical E correlation, which accounts for the effects of the bubble size and the NaOH concentration, was developed.

2. Experimental setup and physical properties

The experimental setup is shown in Fig. 1. An aqueous sodium hydroxide solution was formed inside the enclosed stirrer. In addition to the stirrer, the components of the system used to make the aqueous solution were the glove box, the water tank, and the vacuum pump. NaOH granules (Fuji Film Wako Pure Chemical, 1310-73-2) were first weighed inside the glove box to a predetermined amount. Then purified water (Millipore, Elix Essential UV5) from the tank and the NaOH granules were thoroughly mixed in the stirrer. The concentration of solution was measured by using the pH-meter (TOA DKK, HDM-136A) with uncertainties $\pm$ 0.03 in the pH before entering the lower tank. Argon was used as the purge gas in the tank and the glove box to prevent the reaction of NaOH with CO_2 in the atmosphere.

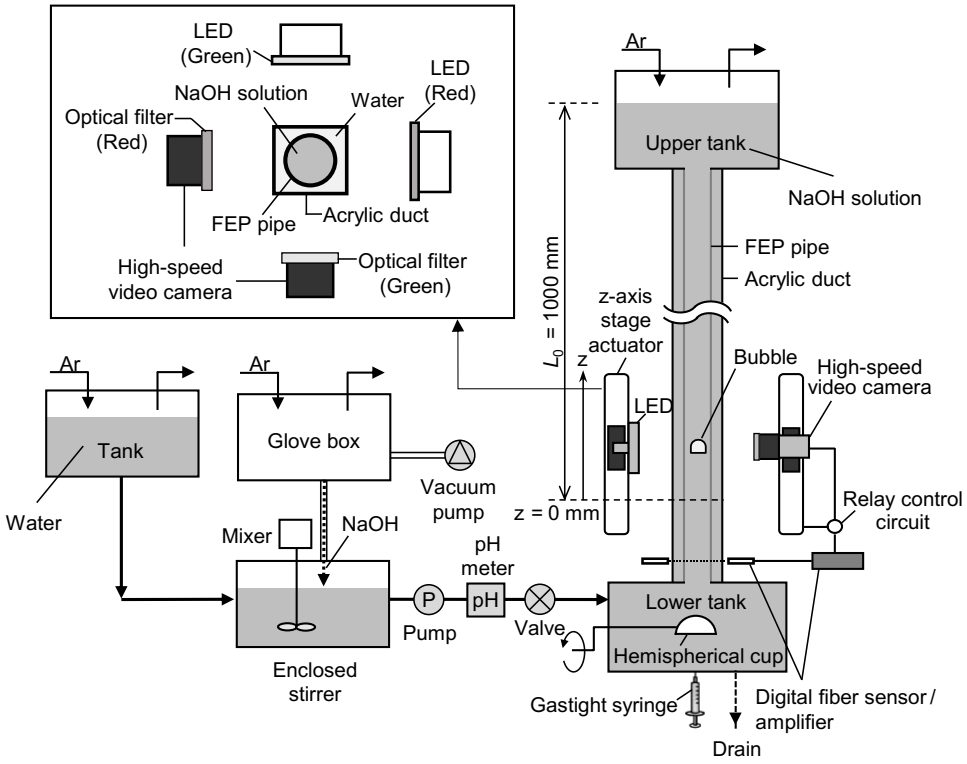

Fig. 1 Experimental setup

The test section consists of the lower tank, the circular pipe, the acrylic duct, the upper tank, the pump, the high-speed video cameras with optical filters, the z-axis stage actuators, the fiber sensor, and

the LED lights. The circular pipe of inner diameter D = 12.5 mm was made of fluorinated ethylene propylene (FEP) resin. The FEP pipe was installed in the acrylic duct and the gap between the pipe and the duct was filled with water. Since the refractive indexes of water and FEP resin are almost equal, 1.333 and 1.338, it is possible to acquire bubble images without any optical distortion. Water in the gap circulated through a water bath tuned at 298 K. All experiments were conducted in room temperature (T = 298 K) and atmospheric pressure ($P \simeq$ 1 atm).

The distance, L_0, from the liquid surface in the upper tank to the reference elevation (z = 0 mm) was 1000 mm. A predetermined amount of CO_2 (Sumitomo Seika, purity 99.9 vol%) gas injected from the bottom of the lower tank was stored in the hemispherical cup by using the gastight syringe and was released by rotating the cup. The NaOH solution was replaced with a fresh one after releasing at most five small bubbles or three Taylor bubbles to avoid the change in the NaOH concentration due to reaction with CO_2. Front and side images of a bubble in the pipe were recorded using the two synchronized video cameras. The green and red LED light sources were used for back illumination. The cameras and the LED light sources were mounted on the actuators, and their movements were synchronized. Bubbles were tracked for $0 \leq z \leq 400$ mm with the video camera setting: 400 frame/s for frame rate, 1000 μs for exposure time, and 0.04-0.05 mm/pixel for spatial resolution. After completion of the experiments and neutralization, the test section and the reactor were cleaned using purified water and k_L^0 of CO_2 in clean water was checked before the next experiments to ensure that all equipment was free from contamination.

Table 1 Gas and liquid properties (T = 298 K, $P \simeq$ 1 atm)

[OH^-] [mol/L]	pH	ρ_L [kg/m^3]	μ_L [10^{-3} Pa·s]	σ [N/m]	D_{CO2} [10^{-9}m^2/s]	C_{sat} [mol/m^3]
10^{-7} (water)	7	997	0.89	0.072	1.92[a]	34.0[b]
0.01	12	998	0.89	0.071	1.92	33.9
0.018	12.25	998	0.90	0.071	1.92	33.8
0.032	12.5	999	0.90	0.071	1.92	33.6
0.063	12.8	1000	0.90	0.070	1.91	33.2
0.08	12.9	1001	0.91	0.070	1.91	33.0
0.1	13	1001	0.91	0.069	1.90	32.7
0.14	13.15	1003	0.92	0.068	1.90	32.2

[a](Himmelblau, 1964)

[b](van Krevelen and Hoftijzer, 1948b)

The physical properties of the liquid and gas phases are shown in Table 1. The liquid density, ρ_L, was measured using a standard hydrometer (JIS B-1525). A tuning fork vibrating viscometer (A&D, SV-A10) was used to measure the liquid viscosity, μ_L. The surface tension, σ, was measured by using the pendant bubble method (Pan et al., 1998). The diffusion coefficient, D_{CO_2}, and the saturated concentration, C_{sat}, of CO_2 in clean water were quoted from Himmelblau (1964) and van Krevelen and Hoftijzer (1948b), respectively. The D_{CO_2} in NaOH solution was calculated with the following approximated equation (Ratcliff and Holdcroft, 1963):

$$D_{CO_2} = D^0_{CO_2}(1 + 0.624 \sum_{i=1}^{m} b_i c_i) \tag{2}$$

where the constants b_i are given in Table 2, c_i [kmol/m^3] is the concentration of ion and m is the total number of ions. The $D^0_{CO_2}$ is the diffusion coefficient of CO_2 in water (Versteeg and van Swaal, 1988) given by

$$D^0_{CO_2} = 2.35 \times 10^{-6} \exp\left(\frac{-2119}{T}\right) \tag{3}$$

The c_i is given by

$$c_i = n_i c_s \tag{4}$$

where n_i is the number of ions and c_s [kmol/m^3] is the concentration of solution. The saturated concentration, C_{sat}, and the Henry constant, H_{CO_2}, are affected by the presence of reactive ions and can be calculated as (Weisenberger and Schumpe, 1996)

$$\log_{10}\left(\frac{C_{sat}}{C_{sat}^0}\right) = \log_{10}\left(\frac{H_{CO_2}^0}{H_{CO_2}}\right) = -\sum_{i=1}^{m}(h_i + h_G)c_i \tag{5}$$

and

$$h_G = h_G^0 + h_T(T - 298.15) \tag{6}$$

where C_{sat}^0 and $H_{CO_2}^0$ are the saturated concentration and the Henry constant of CO_2 in clean water, h_i and h_G are ion-specific and gas-specific parameters, respectively, h_G^0 is the gas-specific parameter for pure gas, and h_T is the gas-specific parameter for the temperature effect. The parameters in Eqs. (5) and (6) are summarized in Table 2. The $H_{CO_2}^0$[Pa] is calculated as a function of temperature (Versteeg and van Swaal, 1988):

$$H_{CO_2}^0 = \frac{1}{3.54 \times 10^{-7}\exp(2044/T)}\frac{\rho_{H2O}}{M_{H2O}} \tag{7}$$

with ρ_{H2O} and M_{H2O} are the water density (997 kg/m^3) and its molar mass (18 g/mol). Note that the calculated values of $D_{CO_2}^0$ and C_{sat}^0 for water using Eqs. (3) and (7) with T = 298 K and P = 1 atm are equal

to the data provided by Himmelblau (1964) and van Krevelen and Hoftijzer (1948b) in Table 1, i.e. $D^0_{CO_2}$ = 1.92×10^{-9} m^2/s and C^0_{sat} = 34.0 mol/m^3. Uncertainties in D_{CO_2} and C_{sat} estimated at 95% confidence were $\pm$0.28% and $\pm$0.42%, respectively.

Table 2 Parameters in Eqs. (2), (5) and (6)

Ion	b_i [m^3/kmol][c]	h_i [m^3/kmol][d]	Gas	$h_G{}^0$ [m^3/kmol][d]	h_T [m^3/(kmol·K)][d]
Na^+	–0.0857	0.1143	CO_2	–0.0172	–0.338 x 10^{-3}
OH^-	–0.1088	0.0839			

[c](Ratcliff, G.A, Holdcroft, 1963)

[d](Weisenberger and Schumpe, 1996)

Bubble volumes, diameters, and positions were measured using an image processing method (Hosoda et al., 2014). The original gray-scale images were transformed into binary images. By assuming that the horizontal cross-sections were elliptical, a three-dimensional bubble shape was reconstructed by piling up the elliptic disks. The sphere-volume-equivalent bubble diameter, d, was evaluated from the volume of the reconstructed bubble shape. The bubble velocities, V_B, were calculated from the rates of change in the axial bubble position. The d ranged from 5 to 17 mm, and therefore, the ranges of the diameter ratio, λ (= d/D), were from 0.4 to 1.4. Since the present experiments dealt with dissolving CO_2 bubbles with volume change, it was difficult to directly estimate the uncertainties in d and V_B. Hosoda et al. (2014) obtained experimental data of d and V_B for 250 air bubbles rising through clean water in the range of $5 \leq d \leq 25$ mm in vertical pipes of D = 12.5, 18.2 and 25.0 mm and showed that the uncertainties in d and V_B estimated at 95% confidence were $\pm$2.1% and $\pm$0.2%, respectively. The present experiment adopted the same method verified by Hosoda et al. for the camera settings such as the spatial resolution of images and the light sources; that is, the uncertainties in d and V in the present experiments are regarded as the same degree as those in their experiments.

The rate of decrease in d was utilized to evaluate k_L and Sh. The rate of change in CO_2 moles inside a bubble is given by

$$\frac{\mathrm{d}n}{\mathrm{d}t} = -k_L A_B (C_{int} - C_0) \tag{8}$$

where n is the moles, t is the time, A_B ($= \pi d^2$) is the bubble surface area, C_0 is the CO_2 concentration in the liquid phase, and C_{int} is the concentration of CO_2 at the bubble interface. The C_0 in Eq. (8) can be neglected since the concentration of CO_2 in the liquid phase is much smaller than C_{int} which is calculated by Henry's law:

$$P(z)X = \frac{C_{int}}{C_{int} + C_V} H_{CO_2} \tag{9}$$

where $P(z)$ is the pressure inside a bubble, X is the mole fraction of CO_2 in the gas phase, which is assumed to be unity, and C_V is the molar concentration of water in the solution (55.4 kmol/m^3). The $P(z)$ is calculated by

$$P(z) = P_{atm} + \rho_L g (L_0 - z) \tag{10}$$

where P_{atm} is the atmospheric pressure, g is the acceleration of gravity, and the surface tension effect in P is small and was neglected in Eq. (10). Substituting Eq. (9) into Eq. (8) yields

$$k_L = -\frac{1}{\pi d^2} \frac{H_{CO2} - P(z)}{C_V P(z)} \frac{\mathrm{d}n}{\mathrm{d}t} \tag{11}$$

The dn/dt can be expressed as the following equation by assuming that CO_2 is an ideal gas:

$$\frac{\mathrm{d}n}{\mathrm{d}t} = \frac{\pi}{6RT}\frac{\mathrm{d}(P(z)d^3)}{\mathrm{d}t} \tag{12}$$

where R is the universal gas constant. The $\mathrm{d}(P(z)d^3)/\mathrm{d}t$ was evaluated as $-(P_2d_2^3 - P_1d_1^3)/(t_2 - t_1)$, where the subscripts 1 and 2 represent the start and end time of a recording period of a single bubble, respectively. The mass transfer coefficient can be evaluated by the following equation:

$$k_L = \frac{(H_{CO2} - P_{12})(P_2d_2^3 - P_1d_1^3)}{6RT(t_2 - t_1)d_{12}^2C_VP_{12}} \tag{13}$$

where the subscript 12 represents the mean value between t_1 and t_2, i.e. $P_{12} = (P_1 + P_2)/2$ and $d_{12} = (d_1 + d_2)/2$.

3. Results and Discussion

3.1 Bubble shape and velocity

The shapes of CO_2 bubbles in water and in the NaOH solution at pH = 13 are compared in Fig. 2(a). Shape oscillation and wobbling motion of ellipsoidal bubbles were observed regardless of the presence of NaOH. The capillary waves are evident at the interface of the semi-Taylor bubbles in both conditions. In water, the Taylor bubble formed at larger λ shows capillary waves in the tail region. Similar capillary waves were observed in the Taylor bubble in the NaOH solution. Hence the presence of NaOH in the solution did not affect the shapes of the bubbles in the present experimental conditions.

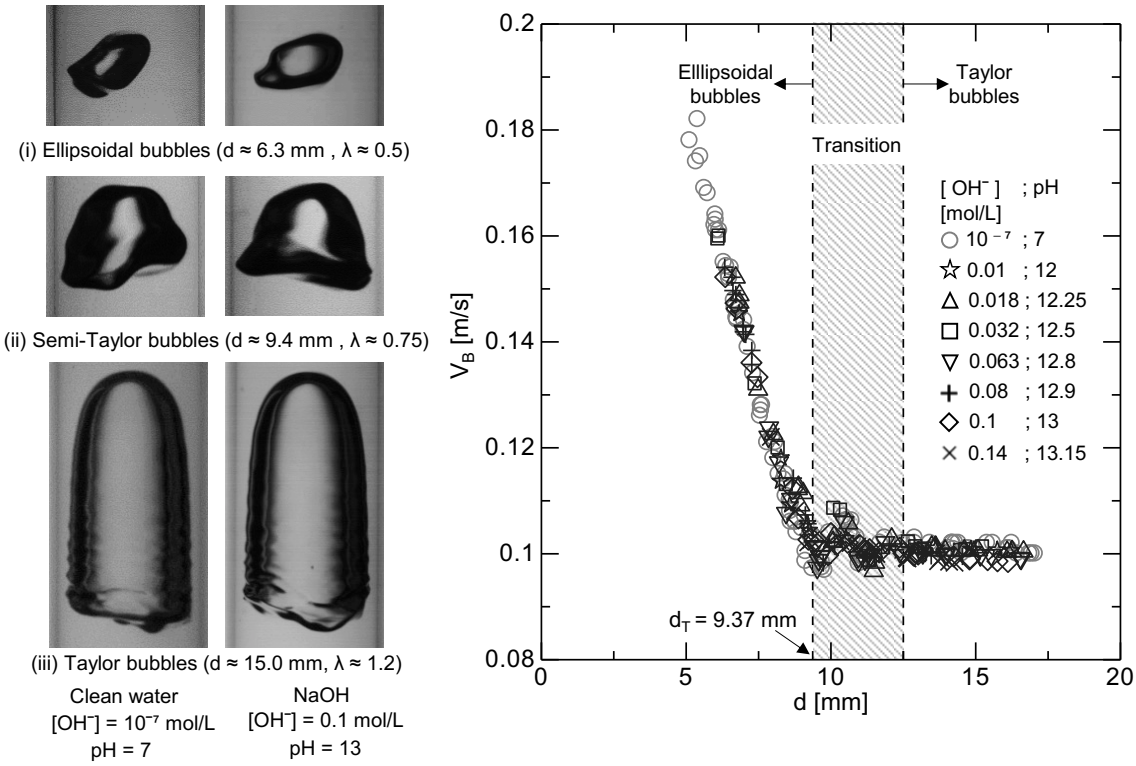

(a) Bubble shape (b) Rise velocity

Fig. 2 Shapes and rise velocities of bubbles

The bubble rise velocity, V_B, is shown in Fig. 2(b). The data are classified into three-regimes: the ellipsoidal, the transition, and the Taylor bubble regimes. In the transition regime, the bubble shape changes from ellipsoidal to Taylor bubble or so-called semi-Taylor bubble as d increases. The d_T in the figure represents the bubble diameter at the transition from ellipsoidal to semi-Taylor bubbles (Aoki et al., 2015a). The V_B in the ellipsoidal bubble regime decreases with increasing d due to the wall effect, while V_B in the Taylor bubble regime is independent of d. A complex dependence of V_B on d is found in the transition regime. The presence of NaOH did not affect V_B for all the regimes. The behavior of bubbles in the present concentrations of the aqueous NaOH solutions, therefore, is similar to that in clean water.

3.2 Mass transfer coefficient and enhancement factor

The mass transfer coefficients for each bubble diameter are shown in Fig. 3. The k_L of ellipsoidal bubbles in clean water (pH = 7) decreases with increasing d, while k_L is nearly constant in the Taylor bubble regime. The k_L at pH = 12 are the same as those at pH = 7, which means that the physical absorption is still dominant over the chemical absorption for pH $\leq$ 12. The ellipsoidal bubbles at pH = 12.25 also have k_L similar to those at pH = 7, while k_L of semi-Taylor and Taylor bubbles at pH = 12.25 are slightly larger than at pH = 12. At higher pH, k_L in the aqueous NaOH solutions increase with increasing pH.

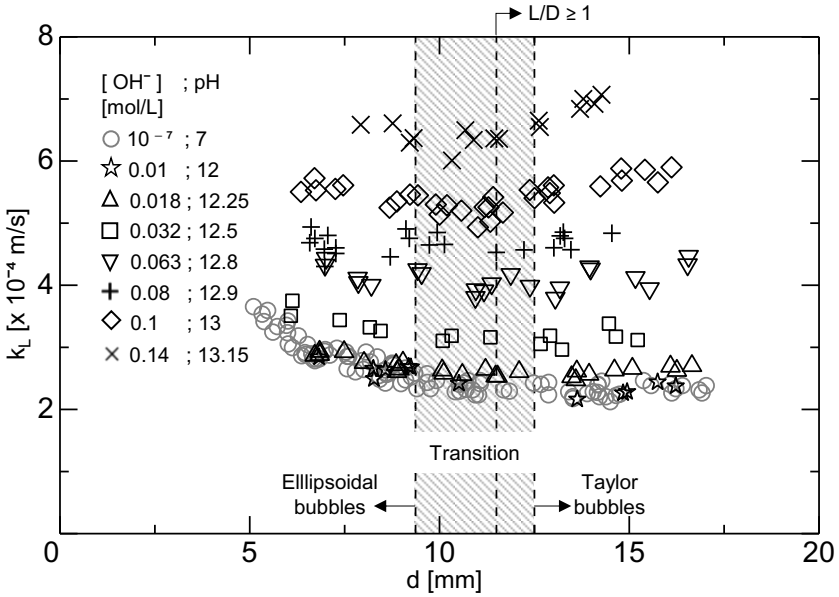

Fig. 3 Mass transfer coefficients of bubbles

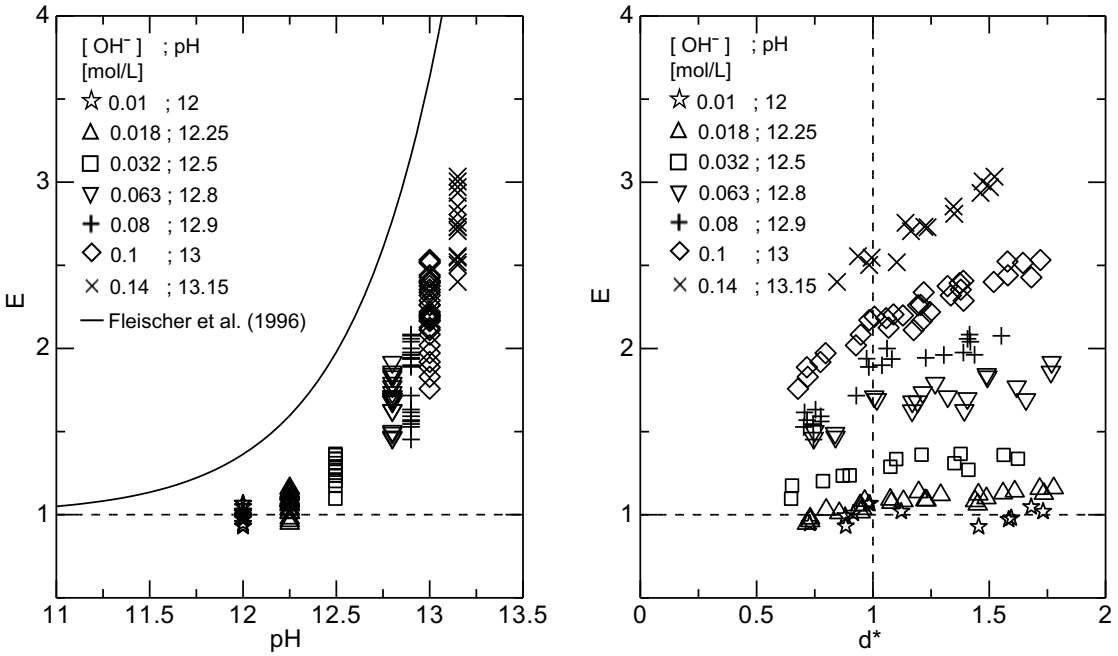

(a) Enhancement factor for each pH (b) Enhancement factor for each d^*

Fig. 4 Enhancement factor

The enhancement factor E shown in Fig. 4 was calculated using k_L of bubbles in the NaOH solution and clean water as defined in Eq. (1). Since it was difficult to obtain k_L and k_L^0 data for the exactly same bubble diameter, a fitting equation of k_L^0 was made using the least-square method (see Appendix A.1). The solid line in Fig. 4(a) represents E predicted by Fleischer et al. (1996). The measured E for pH = 12 is almost unity and much smaller than predicted E (≈ 1.3). Both the measured and predicted E show the same pH dependency, though the measured E is much smaller than the predicted E. As noted before, Fleischer's model is based on the two-film theory for a flat surface. In addition, flow in the vicinity of the interface and interface oscillation present in reality are not accounted for. As shown in Eq. (1), E is defined as the ratio of the mass transfer coefficient in NaOH (k_L) to the mass transfer coefficient in water (k_L^0). In the case of a bubble, the oscillation and capillary wave would enhance diffusion of species in the vicinity of the interface in physical absorption, which contributes to the enhancement of k_L^0. On the other hand, these phenomena are not present in a flat surface. Hence k_L^0 is smaller for a flat surface than for a bubble. This is why the measured E of a bubble is smaller than Fleischer's E. In Fig. 4(b), the measured E is plotted

against d^*, the dimensionless bubble diameter $d^*=d/d_T$. The E increases with increasing d^*. As presumed, the surface area of bubble increases with d^*. Considering physical absorption, dissolved CO_2 at the bubble front region in clean water flows down along the bubble interface and a thin concentration boundary layer of higher CO_2 concentration is formed (Hayashi et al., 2014). The development of the boundary layer, in other words, the attenuation of the concentration gradient at the interface, hinders CO_2 dissolution from the interface except for the front region of a bubble or the wake region where the vortex shedding facilitates the renewal of CO_2 concentration (Hosoda et al. 2015). In NaOH solutions, the CO_2 concentration in the boundary layer is lower due to rapid chemical reaction of CO_2 molecules, which contributes to the increase in CO_2 dissolution (Jia and Zhang, 2017). The mass transfer rate is thus enhanced with increasing the NaOH concentration and the bubble diameter. The increase rate of E with respect to d^* is not constant for all bubble shape regimes, i.e. the increase rate is larger for $d^* < 1$. As shown in Fig. 2(a), the transition of the shape from an ellipsoidal bubble to a semi-Taylor bubble evolves in both radial and axial directions, while that from a semi-Taylor bubble to a Taylor bubble evolves only in the axial direction. The larger increase rate of the interfacial area for $d^* < 1$, therefore, contributes to the larger increase rate of E on d^*.

The following enhancement factor correlation was developed using nonlinear multiple regression with d^* and pH:

$$E = \begin{cases} 1 + \exp(2.98\ \mathrm{pH} + 1.04d^* - 39.7) & \text{for } d^* < 1 \\ 1 + \exp(2.69\ \mathrm{pH} + 0.40d^* - 35.3) & \text{for } 1 \le d^* < 1.8 \end{cases} \tag{14}$$

This correlation consists of two equations to take into account the change in the dependence on d^* at $d^* = 1$ shown in Fig. 4(b). Enhancement factors calculated using Eq. (14) are compared with the data in Fig. 5, which shows good agreement and 93% of the calculated E were within ±10% errors.

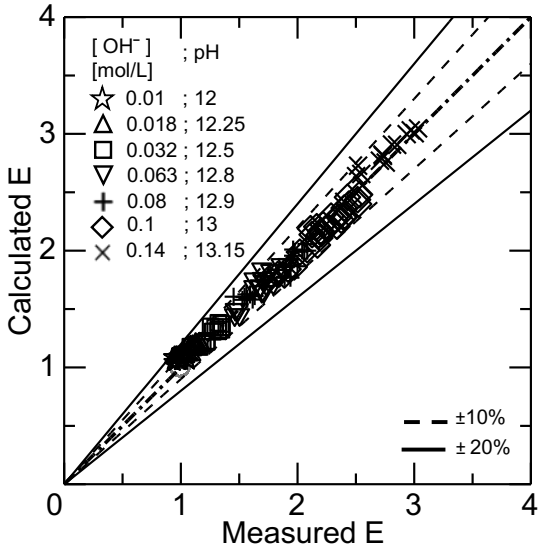

Fig. 5 Measured and calculated *E* using Eq. (14)

The *Sh* of a spherical bubble in clean water can be expressed as $Sh = \alpha Pe^{1/2}$ (Boussinesq, 1905), where α is a constant, *Sh* is defined by

$$Sh = \frac{k_L d}{D_{CO_2}} \tag{15}$$

and *Pe* is the Peclet number defined by

$$Pe = \frac{V_B d}{D_{CO_2}} \tag{16}$$

Based on Boussinesq's relation, Hosoda et al. (2014) proposed an empirical *Sh* correlation for CO_2 bubbles in clean water, in which α is expressed as a function of λ (= *d*/*D*). Hori et al. (2017) pointed out that α cannot be simply expressed as α(λ) and d^* (= d/d_T) is more appropriate for α. This is because d_T increases with decreasing *D*, i.e. λ does not give the same $Sh/Pe^{1/2}$ in the transition regime for different pipe

diameters. Hence, Hori et al. proposed the following correlation applicable to ellipsoidal and semi-Taylor bubbles for $L/D < 1$ in water:

$$Sh^0 = \begin{cases} \frac{2}{\sqrt{\pi}}\left(0.34\, d^{*2} + 0.28 d^* + 1\right)\sqrt{Pe} & \text{for } d^* < 1 \\ (0.18\, d^* + 1.6)\ \sqrt{Pe} & \text{for } d^* \geq 1 \end{cases} \tag{17}$$

where L is the vertical length of a Taylor bubble and d for $L/D = 1$ is in the transition regime (see Fig. 3).

The measured $Sh/Pe^{1/2}$ of ellipsoidal and semi-Taylor bubbles for $L/D < 1$ are plotted against d^* in Fig. 6. The measured data show the increase in $Sh/Pe^{1/2}$ with increasing pH, i.e. the enhancement of mass transfer due to chemical absorption. The values calculated using Eqs. (1), (14) and (17) agree well with the data for each pH and d^*. The comparison between the calculated and measured Sh is also shown in Fig. 7 and 80% of the data are evaluated with errors less than 10%.

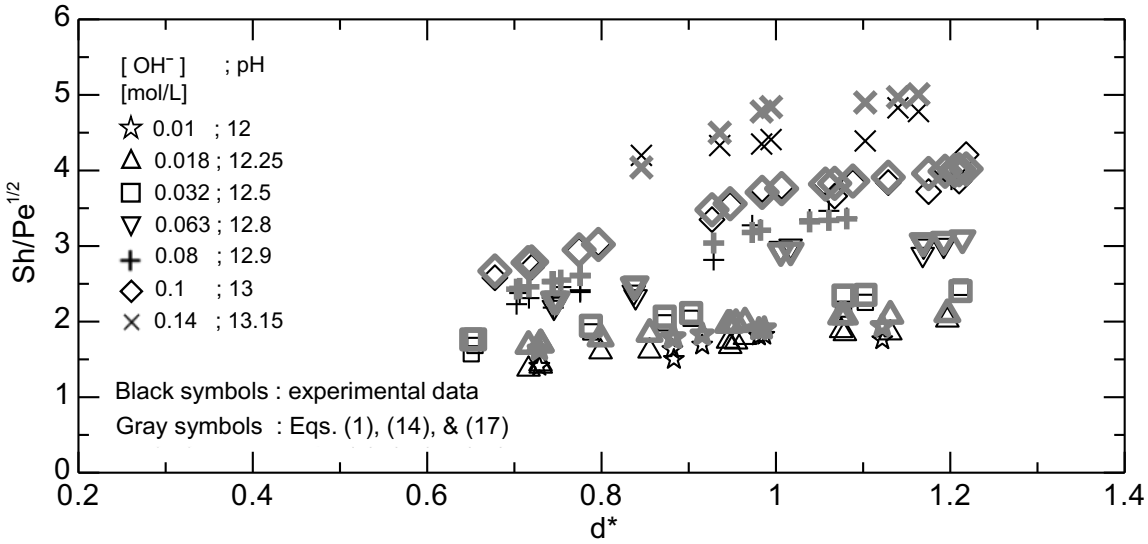

Fig. 6 $Sh/Pe^{1/2}$ vs. d^*

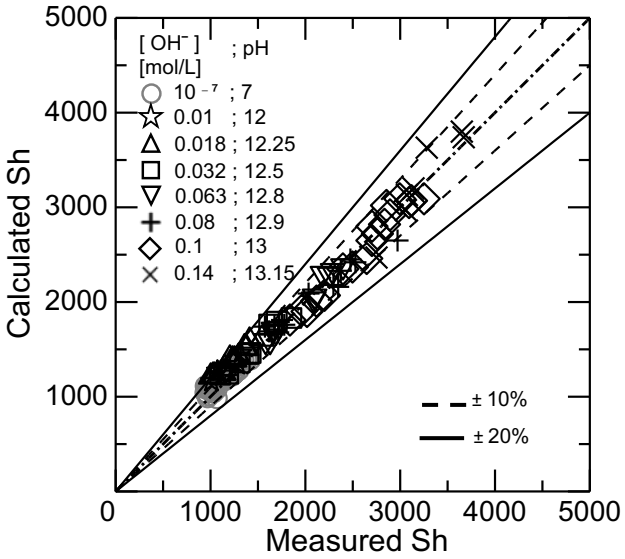

Fig. 7 Comparison between measured and calculated *Sh*

The following Sherwood number correlation for Taylor bubbles of $L/D \geq 1$ in clean water was proposed by Filla (1981):

$$Sh_D^0 = 5.1(L/D)^{0.8}\sqrt{Pe_D} \tag{18}$$

where Sh_D^0 and Pe_D are the modified Sherwood number and the modified Peclet number defined by

$$Sh_D^0 = \frac{k_L A_B}{D_{CO_2} D} \tag{19}$$

and

$$Pe_D = \frac{V_B D}{D_{CO_2}} \quad , \tag{20}$$

respectively. The L/D can be evaluated by using the following correlation proposed by Nakahara and Tomiyama (2003):

$$L/D = (a_1 + 2a_2\lambda + 4a_3\lambda^2)\lambda \tag{21}$$

where the coefficients a_1, a_2 and a_3 are given by

$$\begin{aligned} a_1 &= \min\left(9.39 \times 10^{-5} Re_L + 0.586, 7.20 \times 10^{-6} Re_L + 0.722\right) \\ a_2 &= 5.93 \times 10^{-11} Re_L^2 + 5.95 \times 10^{-7} Re_L - 0.108 \\ a_3 &= -2.06 \times 10^{-7} Re_L + 0.211 \end{aligned} \tag{22}$$

Here Re_L is the liquid Reynold number based on the liquid volumetric flux, which is zero in the present experiment, so that $Re_L = 0$ and Eq. (21) simplifies to

$$L/D = (0.586 - 0.216\lambda + 0.844\lambda^2)\lambda \tag{23}$$

Fig. 8 shows $Sh_D/Pe_D^{1/2}$ plotted against L/D for $L/D \geq 1$. The measured $Sh_D/Pe_D^{1/2}$ increases with increasing pH and L/D. Eq. (18) was combined with the E correlation, Eq. (14), as follows to evaluate the Sherwood number, Sh_D, with chemical absorption:

$$Sh_D = E\, Sh_D^0 \tag{24}$$

This equation can reproduce the dependencies of $Sh_D/Pe_D^{1/2}$ on pH and L/D as can be seen in the comparison between the correlation and the data in Fig. 9, where 74% of the data are to within ±10% errors.

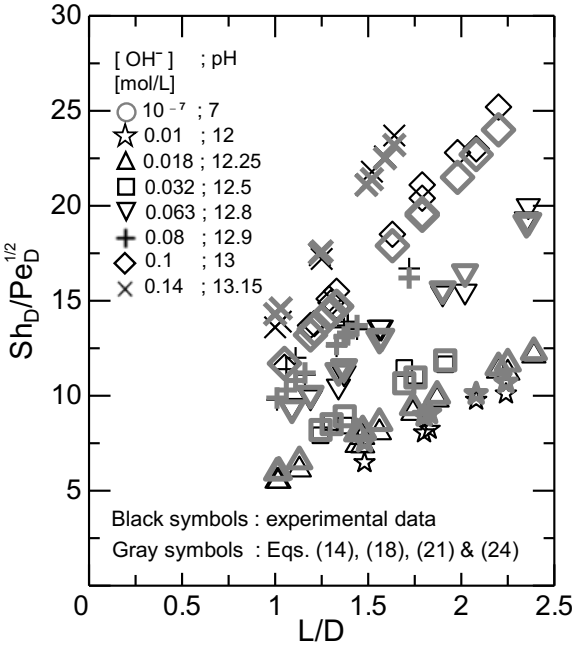

Fig. 8 $Sh_D/Pe_D^{1/2}$ vs. L/D

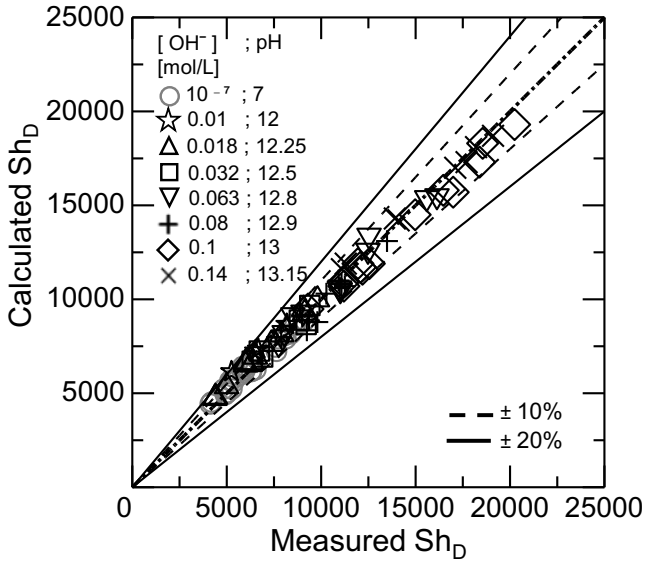

Fig. 9 Comparison between measured and calculated Sh_D

3.3 Applicability of enhancement factor correlation to bubbles in larger pipe diameter

Further observation of bubbles in three different NaOH concentrations in a pipe of D = 18.2 mm was carried out to examine the applicability of the E correlation, Eq. (14), developed for the data of D = 12.5 mm to the larger D. Bubbles at pH = 12.5, 12.8 and 13 have the same V_B as those in clean water as

shown in Fig. 10. The bubble velocity V_B are higher in D = 18.2 mm than in D = 12.5mm since λ are smaller.

The mass transfer coefficients for all bubbles in D = 18.2 mm are shown in Fig. 11, in which the number of the data for $L/D > 1$ is small because of a difficulty in generating large d bubbles in the cup under rapid dissolution especially at high pH .Chemical absorption enhances the mass transfer as in the case of D = 12.5 mm. The tendency of k_L is different with that in D = 12.5 mm; k_L are almost constant in the Taylor bubble regime even at high pH.

The enhancement factors of bubbles in D = 18.2 mm were calculated by comparing k_L in the NaOH solution with approximated k_L^0 which provided by using the least-square method (see Appendix A.2). The measured E are shown in Fig. 12 with the data of D = 12.5 mm, which shows good agreement within the measurement deviation. This result implies that the dependence of the enhancement factor on d is not so much affected by the pipe diameter. Because of high Pe (3.6×10^5–1.4×10^6), the concentration boundary layer forming at the bubble interface is very thin, so that the change in D does not affect the mass transfer in the boundary layer and the pH effect in the Eq. (14) is valid for both D. Though the shape and motion of a bubble are affected by D, the dimensionless diameter d^* can characterize them so that the term d^* in Eq. (14) works well for E as the bubble size effect. The enhancement factor correlation gives good agreement and 91% of the data of D = 18.2 mm lie within $\pm$10% errors as shown in Fig. 13.

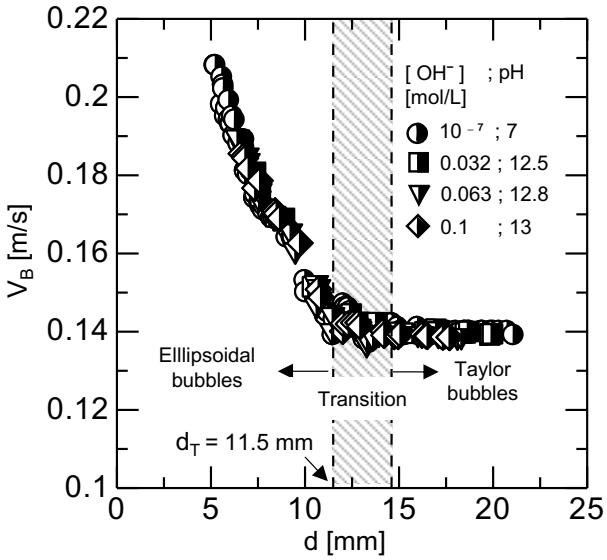

Fig. 10 Rise velocity of bubbles in D = 18.2 mm

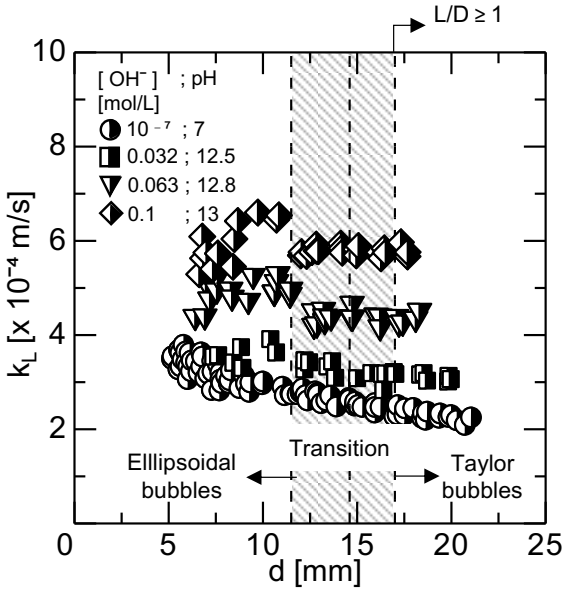

Fig. 11 Mass transfer coefficient of bubbles in D = 18.2mm

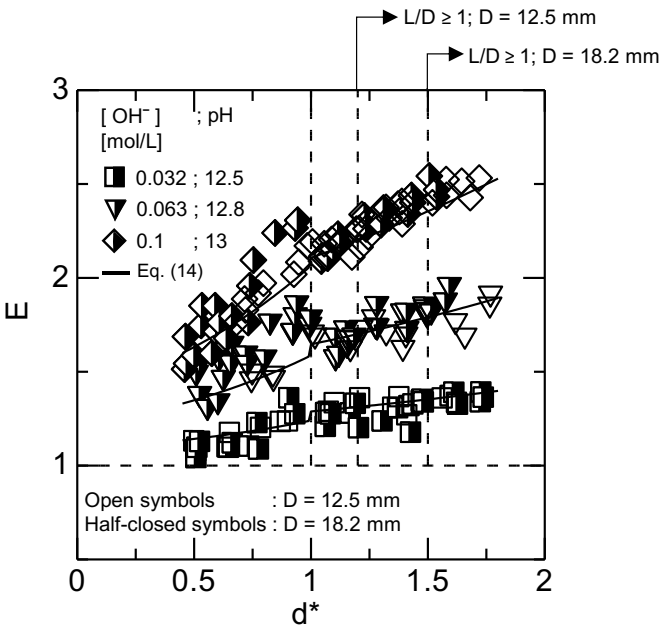

Fig. 12 Enhancement factor for each d^*

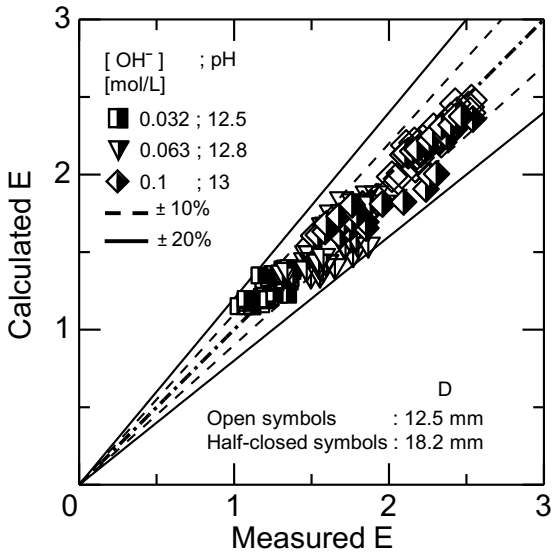

Fig. 13 Measured and calculated E in D = 12.5 and 18.2 mm

Comparison between the *Sh* correlation Eqs. (1), (14) and (17) and the data of D = 18.2 mm is shown in Fig. 14. The dependence of $Sh/Pe^{1/2}$ on d^* is well reproduced by the correlation. As shown in Fig. 15, the *Sh* correlation can evaluate 88% of the data with errors less than ±10%.

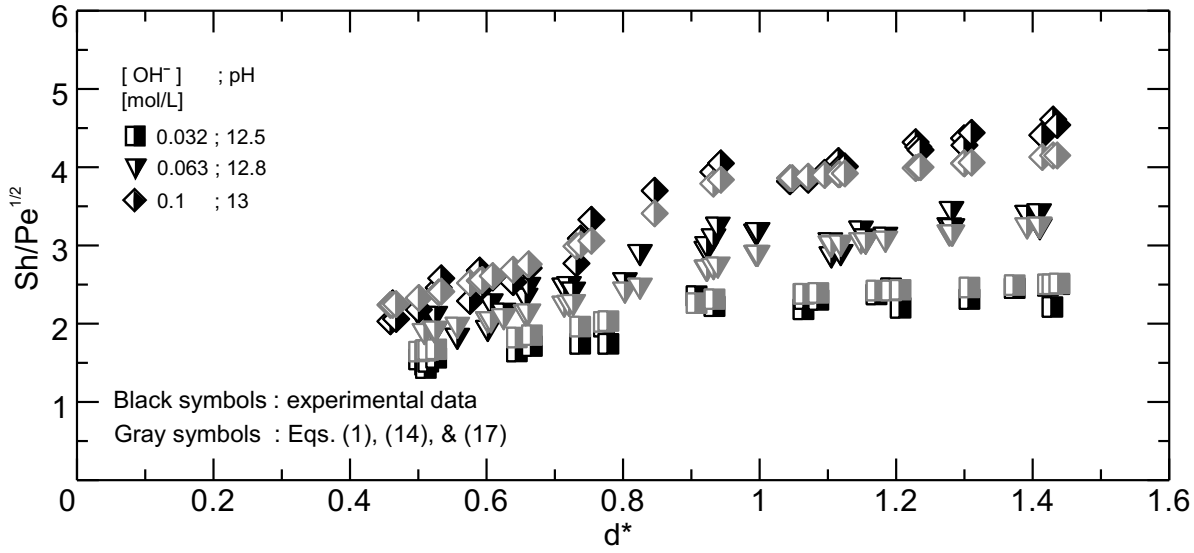

Fig. 14 $Sh/Pe^{1/2}$ vs. d^* (D = 18.2 mm)

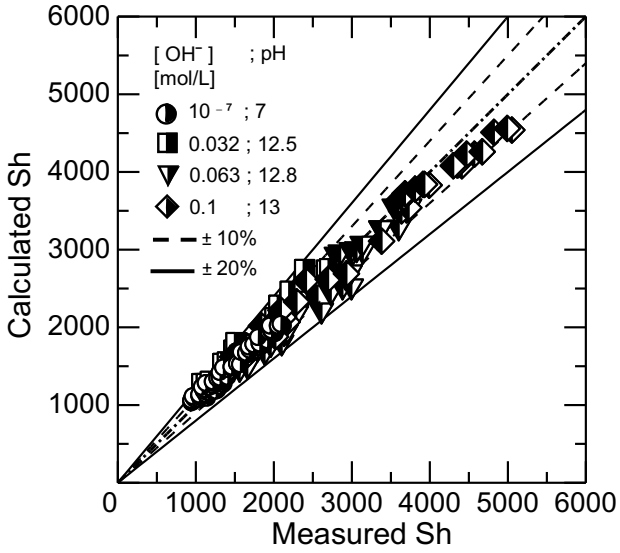

Fig. 15 Measured and calculated Sh in D = 18.2 mm

4. Conclusions

Single CO_2 bubbles rising through a pipe filled with a NaOH solution were measured to understand the effects of pH and the bubble diameter d on the enhancement factor E. The experiments were carried out for a wide range of the dimensionless bubble diameter λ which is the ratio of the bubble diameter to the pipe diameter, $0.4 < \lambda < 1.4$, and for the sodium hydroxide concentration, $12 \leq pH \leq 13.15$. Appendix B tabulates all the data, which would be of use for validation of numerical methods. The conclusions

obtained are as follows:

1. The E for $7 \leq$ pH ≤ 12 is almost unity, i.e. the presence of NaOH does not affect the mass transfer due to low concentration, while the measured E increases with increasing both pH and d for pH $\geq$ 12.25.
2. The enhancement factor model based on the two-film theory and a flat interface (Fleischer et al., 1996) is not applicable to ellipsoidal and Taylor bubbles.
3. The proposed empirical correlation of E for single bubble of $0.4 \leq \lambda \leq 1.4$ and $7 \leq$ pH ≤ 13.15 gave good agreement with 93% of the data within ±10% errors. The correlation was also applicable to D = 18.2 mm.
4. The measured Sherwood numbers can be evaluated by combining the proposed E correlation and available correlations of the Sherwood number without chemical reaction.

Acknowledgement

The authors would like to express their gratitude to Dr. Yohei Hori and Mr. Kanta Sato for his assistance in experiments. This work has been supported by JSPS KAKENHI Grant number 18H03756.

Appendix A :

A.1 k_L^0 in clean water for D = 12.5 mm

Fitting equations of k_L of clean CO_2 bubbles in water are acquired to calculate measured enhancement factors. By using the least-square method, a parabolic curve is fitted for $L/D < 1$ and a constant value is set for $L/D \geq 1$ (Fig. A.1). The equations are expressed as

$$k_L^0 = \begin{cases} 2.45d^2 - 0.06d + 6 \times 10^{-4} & \text{for } L/D < 1 \\ 2.33 \times 10^{-9} & \text{for } L/D \geq 1 \end{cases} \quad \text{(A.1)}$$

where the constants are considered to have the appropriate units so as to make the units of each term [m/s]. The maximum deviation between the equations and the experimental data is 7.75%.

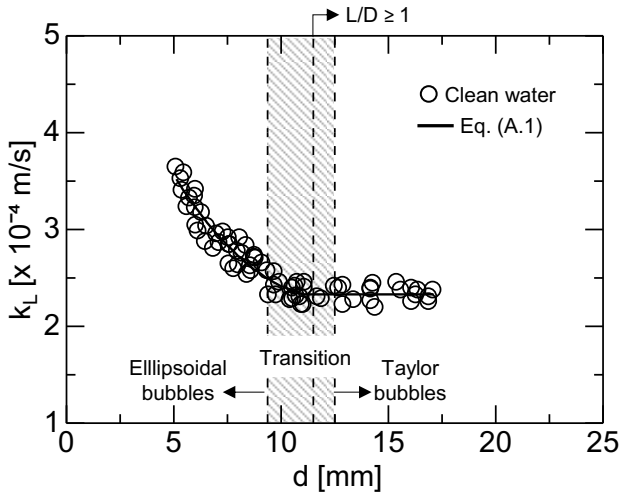

Fig. A.1 Fitting equations of k_L^0 (D = 12.5 mm)

A.2 k_L^0 in clean water for D = 18.2 mm

Being similar to k_L^0 for D = 12.5 mm, k_L^0 for D = 18.2 mm is fitted as

$$k_L^0 = 0.36d^2 - 0.017d + 4 \times 10^{-4} \quad \text{(A.2)}$$

The maximum deviation between the equation and the experimental data is 14%.

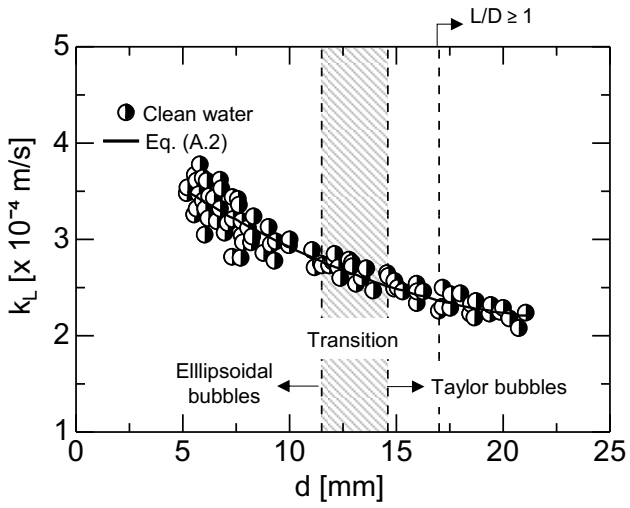

Fig. A.2 Fitting equation of k_L^0 (D = 18.2 mm)

Appendix B : Experimental data

Table B.1 Experimental data for D = 12.5 mm*

d	V_B	k_L	d	V_B	k_L	d	V_B	k_L	d	V_B	k_L	d	V_B	k_L
Clean water			10.56	0.106	2.28	pH = 12.25			7.86	0.124	4.05	7.25	0.136	5.55
5.12	0.178	3.64	10.67	0.104	2.41	6.71	0.152	2.87	9.42	0.101	4.25	7.46	0.133	5.61
5.35	0.174	3.52	10.72	0.106	2.31	6.84	0.147	2.93	9.53	0.097	4.19	8.68	0.112	5.25
5.40	0.182	3.40	10.77	0.103	2.45	6.84	0.149	2.88	10.95	0.099	3.81	8.88	0.107	5.35
5.49	0.175	3.58	10.89	0.103	2.30	7.49	0.131	2.93	10.96	0.099	3.93	9.22	0.103	5.46
5.63	0.169	3.23	10.97	0.098	2.22	8.01	0.123	2.75	11.17	0.099	3.91	9.43	0.102	5.45
5.75	0.168	3.32	11.05	0.100	2.22	8.86	0.112	2.72	11.37	0.100	4.03	9.90	0.100	5.30
5.99	0.162	3.34	11.10	0.099	2.45	8.88	0.113	2.61	11.88	0.102	4.17	10.00	0.104	5.14
6.02	0.164	3.22	11.10	0.100	2.40	8.94	0.109	2.65	12.38	0.100	3.99	10.20	0.102	5.29
6.03	0.163	3.41	11.71	0.102	2.30	9.04	0.111	2.76	13.05	0.101	3.79	10.58	0.102	5.20
6.04	0.161	3.04	11.87	0.103	2.28	10.07	0.102	2.63	13.17	0.100	3.96	11.01	0.102	4.93
6.15	0.161	2.98	12.50	0.102	2.41	10.11	0.103	2.58	13.95	0.100	4.30	11.19	0.101	5.26
6.31	0.155	3.17	12.70	0.102	2.39	10.60	0.106	2.56	13.98	0.100	4.26	11.29	0.100	5.25
6.49	0.152	2.87	12.90	0.102	2.22	11.21	0.100	2.64	15.16	0.100	4.13	11.34	0.101	5.02
6.55	0.154	3.03	12.90	0.103	2.42	11.48	0.097	2.53	15.54	0.100	3.95	11.41	0.099	5.42
6.86	0.146	2.80	13.43	0.102	2.27	11.53	0.098	2.53	16.54	0.099	4.33	11.67	0.100	5.17
7.01	0.144	2.95	14.18	0.102	2.26	12.10	0.103	2.61	16.57	0.099	4.47	12.38	0.101	5.53
7.13	0.139	2.86	14.20	0.102	2.38	13.48	0.101	2.52	pH = 12.9			12.50	0.100	5.40
7.32	0.134	2.97	14.20	0.102	2.39	13.59	0.101	2.48	6.58	0.152	4.69	12.86	0.100	5.58
7.56	0.126	2.91	14.30	0.102	2.44	13.62	0.101	2.62	6.62	0.150	4.94	12.91	0.100	5.48
7.59	0.128	2.64	14.41	0.102	2.19	13.94	0.101	2.56	6.72	0.149	4.75	13.01	0.100	5.61
7.60	0.127	2.84	15.40	0.102	2.45	14.61	0.101	2.63	6.96	0.143	4.58	13.02	0.100	5.33
7.63	0.128	2.84	15.60	0.102	2.37	15.08	0.101	2.66	6.98	0.142	4.30	14.24	0.100	5.59
7.81	0.121	2.59	16.10	0.101	2.39	16.09	0.100	2.69	7.06	0.141	4.80	14.79	0.099	5.88
7.98	0.122	2.77	16.15	0.101	2.25	16.25	0.100	2.63	7.27	0.136	4.51	14.80	0.099	5.68
8.02	0.118	2.63	16.25	0.102	2.32	16.65	0.100	2.70	7.27	0.138	4.60	15.41	0.099	5.86
8.09	0.121	2.91	16.42	0.100	2.37	pH = 12.5			8.70	0.114	4.46	15.75	0.099	5.66
8.20	0.115	2.75	16.86	0.100	2.30	6.11	0.159	3.49	9.12	0.107	4.91	16.11	0.098	5.90
8.39	0.114	2.83	16.94	0.100	2.25	6.15	0.160	3.73	9.20	0.106	4.76	pH = 13.15		
8.43	0.115	2.53	17.05	0.100	2.37	7.39	0.132	3.42	9.73	0.098	4.65	7.92	0.122	6.58
8.59	0.110	2.62	pH = 12			8.19	0.120	3.31	9.94	0.102	4.85	8.77	0.108	6.61
8.62	0.106	2.57	6.83	0.145	2.84	8.47	0.113	3.25	10.13	0.101	4.66	9.22	0.102	6.30
8.77	0.106	2.71	8.26	0.114	2.66	10.11	0.109	3.09	11.50	0.099	4.53	9.32	0.103	6.37
8.78	0.106	2.73	8.27	0.118	2.49	10.34	0.108	3.17	12.23	0.101	4.57	10.33	0.102	6.01
8.82	0.104	2.70	8.58	0.109	2.64	11.37	0.099	3.15	13.01	0.101	4.60	10.68	0.102	6.50
9.13	0.099	2.65	9.19	0.106	2.69	12.69	0.102	3.04	13.18	0.100	4.80	10.90	0.101	6.34
9.37	0.097	2.57	9.24	0.104	2.68	12.94	0.101	3.17	13.26	0.100	4.86	11.44	0.100	6.37
9.43	0.103	2.32	10.51	0.103	2.42	13.25	0.101	2.95	13.29	0.100	4.75	11.57	0.100	6.36
9.69	0.098	2.56	13.63	0.101	2.16	14.67	0.101	3.16	13.46	0.100	4.57	12.61	0.099	6.65
9.70	0.097	2.42	14.84	0.101	2.26	15.25	0.101	3.10	14.54	0.100	4.84	12.64	0.099	6.55
9.78	0.097	2.32	14.94	0.101	2.28	pH = 12.8			pH = 13			13.70	0.099	6.84
9.94	0.104	2.45	15.75	0.101	2.44	6.98	0.142	4.33	6.35	0.152	5.50	13.79	0.099	7.00
10.44	0.107	2.27	16.22	0.101	2.38	7.01	0.142	4.44	6.71	0.147	5.72	14.08	0.098	6.92
10.55	0.106	2.39				7.84	0.122	4.12	6.74	0.146	5.53	14.27	0.098	7.07

Table. B.2 Experimental data for D = 18.2 mm*

d	V_B	k_L	d	V_B	k_L	d	V_B	k_L	d	V_B	k_L	d	V_B	k_L
Clean water			11.10	0.144	2.88	21.10	0.139	2.23	18.58	0.139	3.17	18.31	0.139	4.52
5.23	0.208	3.47	11.21	0.145	2.70	21.39	0.140	2.13	18.77	0.140	3.01	pH = 13		
5.26	0.208	3.53	11.51	0.139	2.74	21.50	0.139	2.21	19.89	0.139	2.99	5.28	0.189	5.28
5.58	0.198	3.25	11.56	0.143	2.72	21.79	0.140	2.14	19.92	0.139	3.11	5.32	0.189	5.88
5.61	0.205	3.66	11.90	0.144	2.72	21.90	0.140	2.19	20.03	0.139	3.04	5.38	0.192	5.37
5.69	0.203	3.60	12.07	0.147	2.76	22.70	0.140	2.09	pH = 12.8			5.76	0.188	5.44
5.69	0.202	3.31	12.14	0.146	2.77	22.77	0.138	2.32	5.85	0.194	5.11	6.10	0.185	5.91
5.79	0.195	3.46	12.15	0.146	2.84	22.91	0.140	2.15	6.02	0.188	4.69	6.14	0.189	6.25
5.84	0.197	3.77	12.33	0.146	2.70	23.05	0.140	2.07	6.04	0.193	5.27	6.62	0.186	5.29
5.98	0.199	3.63	12.42	0.145	2.59	23.28	0.140	2.16	6.41	0.190	4.39	6.79	0.185	6.09
5.99	0.194	3.39	12.83	0.141	2.78	23.36	0.140	2.25	6.92	0.185	4.40	6.83	0.184	5.63
6.07	0.193	3.04	12.97	0.140	2.75	24.31	0.140	2.24	6.97	0.184	5.14	7.01	0.182	5.75
6.10	0.193	3.31	12.98	0.140	2.71	24.32	0.140	2.23	7.19	0.181	4.76	7.35	0.177	5.40
6.17	0.195	3.60	13.16	0.138	2.53	24.52	0.140	2.19	7.56	0.174	4.95	7.61	0.179	5.73
6.24	0.190	3.21	13.42	0.137	2.59	24.91	0.139	2.25	7.61	0.176	5.26	8.42	0.171	5.45
6.28	0.194	3.44	13.63	0.140	2.69	pH = 12.5			8.21	0.170	4.96	8.49	0.170	6.04
6.50	0.188	3.42	13.96	0.142	2.46	5.78	0.192	3.86	8.29	0.170	4.97	8.67	0.169	6.42
6.64	0.189	3.18	14.62	0.142	2.64	5.89	0.192	3.66	8.36	0.169	4.80	9.73	0.163	6.60
6.79	0.187	3.61	14.66	0.142	2.61	5.90	0.191	3.53	9.23	0.166	4.73	10.72	0.151	6.45
6.79	0.189	3.31	14.94	0.140	2.48	5.94	0.189	3.71	9.49	0.161	5.26	10.85	0.149	6.54
6.85	0.181	3.52	14.95	0.141	2.56	6.07	0.189	3.80	10.60	0.153	4.90	12.01	0.140	5.69
7.01	0.180	3.06	15.11	0.140	2.49	7.43	0.181	3.52	10.62	0.147	4.91	12.05	0.142	5.76
7.15	0.181	3.16	15.34	0.139	2.45	7.69	0.174	3.55	10.72	0.151	5.13	12.32	0.142	5.68
7.35	0.174	2.81	16.00	0.140	2.53	8.50	0.169	3.39	10.80	0.148	5.30	12.60	0.142	5.76
7.38	0.175	3.43	16.00	0.140	2.33	8.90	0.168	3.72	11.44	0.140	4.86	12.83	0.142	5.92
7.39	0.178	3.20	16.01	0.141	2.45	8.97	0.169	3.28	11.47	0.144	4.97	12.85	0.142	5.79
7.62	0.173	3.41	16.30	0.140	2.45	10.46	0.151	3.89	12.69	0.143	4.51	12.94	0.141	5.78
7.68	0.172	3.35	17.03	0.140	2.25	10.76	0.150	3.61	12.71	0.141	4.20	14.13	0.140	5.94
7.75	0.172	2.80	17.20	0.140	2.29	12.26	0.144	3.25	12.87	0.141	4.23	14.18	0.140	5.84
7.80	0.172	3.18	17.21	0.139	2.49	12.27	0.143	3.44	13.21	0.138	4.54	14.21	0.139	5.75
7.80	0.171	3.03	17.57	0.139	2.28	12.51	0.144	3.40	13.28	0.137	4.30	14.94	0.139	5.82
7.87	0.172	2.96	17.60	0.140	2.42	13.49	0.138	3.31	13.29	0.138	4.40	14.95	0.139	5.69
8.10	0.170	3.11	18.04	0.140	2.43	13.74	0.140	3.42	13.62	0.139	4.38	15.07	0.139	5.89
8.24	0.169	2.96	18.50	0.140	2.22	13.90	0.142	3.07	14.70	0.139	4.38	16.26	0.139	5.63
8.29	0.171	3.02	18.55	0.140	2.32	15.06	0.140	3.06	14.73	0.139	4.67	16.45	0.139	5.84
8.36	0.169	3.23	18.70	0.140	2.18	15.82	0.139	3.17	14.75	0.139	4.37	16.51	0.139	5.75
8.82	0.169	2.85	18.77	0.140	2.35	16.38	0.139	3.15	16.01	0.139	4.42	17.33	0.139	5.97
9.06	0.164	3.12	19.42	0.140	2.22	16.45	0.140	2.81	16.21	0.139	4.40	17.68	0.139	5.67
9.17	0.166	2.94	19.47	0.140	2.31	16.57	0.139	3.16	16.22	0.139	4.17	17.68	0.139	5.76
9.33	0.164	2.77	19.90	0.140	2.24	16.98	0.140	3.17	17.09	0.139	4.39			
9.40	0.164	2.97	20.04	0.140	2.28	17.01	0.140	3.19	17.22	0.139	4.25			
10.02	0.153	2.93	20.34	0.140	2.17	17.08	0.140	3.15	17.42	0.139	4.27			
10.05	0.150	2.99	20.78	0.140	2.07	18.41	0.139	3.14	18.11	0.139	4.35			

*the units of d, V_B, and k_L are mm, m/s, and (x 10^{-4}) m/s, respectively.

Presented experimental data of clean water were provided from our previous study (Hosoda et al., 2014; Aoki et al., 2015b).

References

Aoki, J., Hayashi, K., Hosokawa, S., Tomiyama, A., 2015a. Effects of surfactants on mass transfer from single carbon dioxide bubbles in vertical pipes. Chemical Engineering and Technology 38, 1955–1964.

Aoki, J., Hayashi, K., Tomiyama, A., 2015b. Mass transfer from single carbon dioxide bubbles in contaminated water in a vertical pipe. International Journal of Heat and Mass Transfer 83, 652–658.

Boussinesq, J., 1905. Calcul du pouvoir refroidissant des fluides. J. Math. 1, 285–332.

Brian, P.L.T., Hurley, J.F., Hasseltine, E.H., 1961. Penetration theory for gas absorption accompanied by a second order chemical reaction. AIChE Journal 7, 226–231.

Danckwerts, P. V., 1970. Gas-Liquid Reactions: McGraw-Hill, New York.

Darmana, D., Deen, N.G., Kuipers, J.A.M., 2005. Detailed modeling of hydrodynamics, mass transfer and chemical reactions in a bubble column using a discrete bubble model. Chemical Engineering Science 60, 3383–3404.

Darmana, D., Henket, R.L.B., Deen, N.G., Kuipers, J.A.M., 2007. Detailed modelling of hydrodynamics, mass transfer and chemical reactions in a bubble column using a discrete bubble model: Chemisorption of CO_2 into NaOH solution, numerical and experimental study. Chemical Engineering Science 62, 2556–2575.

DeCoursey, W.J., 1974. Absorption with chemical reaction: development of a new relation for the Danckwerts model. Chemical Engineering Science 29, 1867–1872.

Filla, M., 1981. Gas absorption from a slug held stationary in downflowing liquid. The Chemical Engineering Journal 22, 213–220.

Fleischer, C., Becker, S., Eigenberger, G., 1996. Detailed modeling of the chemisorption of CO_2 into NaOH in a bubble column. Chemical Engineering Science 51, 1715–1724.

Hayashi, K., Hosoda, S., Tryggvason, G., Tomiyama, A., 2014. Effects of shape oscillation on mass transfer from a Taylor bubble. International Journal of Multiphase Flow 58, 236–245.

Hikita, H., Asai, S., 1976. Gas absorption with a two-step chemical reaction. The Chemical Engineering Journal 11,

123–129.

Hikita, H., Asai, S., Takatsuka, T., 1972. Gas absorption with a two-step instantaneous chemical reaction. The Chemical Engineering Journal 4, 31–40.

Himmelblau, D.M., 1964. Diffusion of dissolved gases in liquids. Chemical Reviews 64, 527–550.

Hori, Y., Hayashi, K., Hosokawa, S., Tomiyama, A., 2017. Mass transfer from single carbon-dioxide bubbles in electrolyte aqueous solutions in vertical pipes. International Journal of Heat and Mass Transfer 115, 663–671.

Hosoda, S., Abe, S., Hosokawa, S., Tomiyama, A., 2014. Mass transfer from a bubble in a vertical pipe. International Journal of Heat and Mass Transfer 69, 215–222.

Hosoda, S., Tryggvason, G., Hosokawa, S., Tomiyama, A., 2015. Dissolution of single carbon dioxide bubbles in a vertical pipe. Journal of Chemical Engineering of Japan 48, 418–426.

Jia, H.W., Zhang, P., 2017. Mass transfer of a rising spherical bubble in the contaminated solution with chemical reaction and volume change. International Journal of Heat and Mass Transfer 110, 43–57.

Krauß, M., Rzehak, R., 2018. Reactive absorption of CO_2 in NaOH: An Euler-Euler simulation study. Chemical Engineering Science 181, 199–214.

Krauβ, M., Rzehak, R., 2017. Reactive absorption of CO_2 in NaOH: Detailed study of enhancement factor models. Chemical Engineering Science 166, 193–209.

Kundu, A., Basu, J.K., Das, G., 2012. A novel gas-liquid contactor for chemisorption of CO_2. Separation and Purification Technology 94, 115–123.

Madhavi, T., Golder, A.K., Samanta, A.N., Ray, S., 2007. Studies on bubble dynamics with mass transfer. Chemical Engineering Journal 128, 95–104.

Mondal, M.K., Balsora, H.K., Varshney, P., 2012. Progress and trends in CO_2 capture/separation technologies: A review. Energy 46, 431–441.

Nakahara, Y., Tomiyama, A., 2003. Shapes and rising velocities of single bubbles in vertical pipes. Trans. Jpn. Soc. Mech. Eng. B 69, 2001–2009.

Pan, R., Green, J., Maldarelli, C., 1998. Theory and experiment on the measurement of kinetic rate constants for

surfactant exchange at an air/water interface. Journal of Colloid and Interface Science 205, 213–230.

Peng, Y., Zhao, B., Li, L., 2012. Advance in Post-Combustion CO_2 Capture with Alkaline Solution: A Brief Review. Energy Procedia 12, 1515–1522.

Ratcliff, G.A, Holdcroft, J.G., 1963. Diffusivities of gases in aqueous electrolyte solutions. Transactions of the Institution of Chemical Engineers 41, 315–319.

Schulzke, T., Schlüter, S., Weinspach, P.M., 1998. Experimental studies and simulation of the dynamic behaviour of bubble column reactors. Computers and Chemical Engineering 22, S667–S670.

Shim, J.G., Lee, D.W., Lee, J.H., Kwak, N.S., 2016. Experimental study on capture of carbon dioxide and production of sodium bicarbonate from sodium hydroxide. Environmental Engineering Research 21, 297–303.

Sujatha, K.T., Jain, D., Kamath, S., Kuipers, J.A.M., Deen, N.G., 2017. Experimental and numerical investigation of a micro-structured bubble column with chemisorption. Chemical Engineering Science 169, 225–234.

van Krevelen, D.W., Hoftijzer, P.J., 1948a. Kinetics of gas-liquid reactions part I. General theory. Recueil des Travaux Chimiques des Pays-Bas 67, 563–586.

van Krevelen, D.W., Hoftijzer, P.J., 1948b. Sur la solubilite des gaz dans les solutions aqueouses. Ind. 21st Congr. Int. Chim. Ind., 168.

Versteeg, G.F., van Swaal, W.P.M., 1988. Solubility and diffusivity of acid gases (CO_2, N_2O) in aqueous alkanolamine solutions. Journal of Chemical and Engineering Data 33, 29–34.

Weisenberger, S., Schumpe, A., 1996. Estimation of gas solubilities in salt solutions at temperatures from 273 K to 363 K. AIChE Journal 42, 298–300.